Mid/far-infrared photo-detectors based on graphene asymmetric quantum wells

E Ben Salem[1,2,†], R Chaabani[2], and S Jaziri[2,3]

[1] *Institut Préparatoire aux Etudes d'Ingénieurs de Tunis, 2, Rue Jawaher Lel Nahrou Monfleury* 1089, *Tunisie*
[2] *Laboratoire de Physique de la Matière Condensée, Département de Physique, Faculté des Sciences de Tunis, Campus Universitaire* 2092, *Tunisie*
[3] *Département de Physique, Faculté des Sciences de Bizerte, Jarzouna* 7021, *Bizerte*

(Received 19 December 2015; revised manuscript received 18 April 2016; published online 19 July 2016)

We conducted a theoretical study on the electronic properties of a single-layer graphene asymmetric quantum well. Quantification of energy levels is limited by electron–hole conversion at the barrier interfaces and free-electron continuum. Electron–hole conversion at the barrier interfaces can be controlled by introducing an asymmetry between barriers and taking into account the effect of the interactions of the graphene sheet with the substrate. The interaction with the substrate induces an effective mass to carriers, allowing observation of Fabry–Pérot resonances under normal incidence and extinction of Klein tunneling. The asymmetry, between barriers creates a transmission gap between confined states and free-electron continuum, allowing the large graphene asymmetric quantum well to be exploited as a photo-detector operating at mid- and far-infrared frequency regimes.

Keywords: graphene, quantum wells, reflection coefficient, photo-detector

PACS: 81.05.ue, 81.07.St, 78.20.Ci, 85.60.Gz **DOI:** 10.1088/1674-1056/25/9/098101

1. Introduction

Due to its special fundamental properties[1–4] and potential applications in the fields of nanoelectronics, optoelectronics, spintronics, and sensors,[5–13] graphene has attracted enormous scientific and technological interest. Faced with its properties such as sensitivity to the entire ultraviolet to far-infrared range light[14,15] that offer a multitude of application possibilities,[16,17] some are looking for graphene photo-detectors operating at different wavelength regimes.[18,19] Thus graphene nanostructures of reduced dimensionality, such as quantum wells and quantum dots, are very interesting systems for the study of fundamental physical phenomena for photo-detectors and photo-voltaic cells.

Due to the chiral nature of quasi-particles, quantum tunneling in graphene becomes highly anisotropic and qualitatively different from the case of non-relativistic electrons, and strongly affects the transport properties.[20] Limitations encountered for graphene are essentially the zero gap, the very weak spin–orbit coupling, and the absence of hyperfine interaction.[21] The fundamental problem to be solved is the ability to make semiconductor tunable gaps and lift the degeneracy of valleys K and K' in order to remove transmission via the Klein tunneling process. Several schemes have been proposed to overcome this problem such as single-layer strips, gated nanoribbons, gated and/or doped bilayers, etc.[22,23] In this work, we confine electrons in monolayer graphene by imposing a confining potential using the "split gate technology".[24,25] The graphene sheet is coupled to a substrate which has a wide gap and a structure similar to that of graphene with a lattice parameter difference less than $4^\circ/^\circ$.[26] The stable configuration of a graphene sheet on the top of hexagonal boron nitride h-BN (Cu) induces an energy gap of 53 meV (9 meV).[27–29] The presence of the substrate causes the appearance of electron–hole puddles, leading to the fluctuation of the Fermi energy near the Dirac point,[30–32] which limits the device performance. The disorder strength depends strongly on the substrate and the Fermi energy of the electron–hole puddles reaches 55.6 meV for the SiO_2 substrate.[33] Until now, the experimental results have shown that h-BN is the most appealing substrate which offers high quality graphene devices.[33,34] Indeed, the Fermi energy of the electron–hole puddles induced by the h-BN substrate is about 5.4 meV.[33] As the Fermi energy remains sufficiently larger than that corresponding to the puddles, the graphene sheet is considered to be perfect and the effect of the electron–hole puddles can be neglected.

The previous theoretical studies on relativistic fermions have indicated that the nature of electron states in graphene quantum wells differs considerably from that of the non-relativistic case.[22] Relativistic electrons in the quantum well have two essential properties. First, the confined state presents an unusual quasi-linear dependence on the free component of the wave vector and the quantification of the energy levels is limited by the electron–hole conversion at the barrier interfaces due to the Klein tunneling of electrons to holes outside the potential well.[22] Second, there is a constructive interfer-

†Corresponding author. E-mail: bensalem_emna@yahoo.fr

© 2016 Chinese Physical Society and IOP Publishing Ltd

ence between confined states and free states at the edge of the free electron continuum.[22] Hence we are interested to find the scattering mechanisms that may occur in a quantum well of graphene. Mhamdi *et al.*[35] deepened the study of the back-scattering caused by the action of the potential well on the charge carriers.

Wang *et al.*[36] presented a theoretical study of the quantum well based on graphene and narrow semiconductors with two different energy gaps. They proposed to use graphene quantum wells to fabricate photovoltaic cells.[36] In this case, the effect of the effective mass induced by the coupling with the substrate is not important and does not affect the energy spectrum. Questions that arise here are can this theoretical model be extended to low energy regimes, namely, mid- and far-infrared frequency regimes, and what is the physical quantity that proves this model can be applied to fabricate photovoltaic cells and mid/far-infrared photo-detectors.

To respond to these questions, we present in this paper a theoretical study on graphene quantum wells based on low Fermi energies (< 1 eV). We show that in such systems, the electron–hole conversion at the barrier interfaces can be controlled by introducing an asymmetry between the barriers and taking into account the coupling of the graphene sheet with the substrate, thereby controlling the number of quantized energy levels near the Dirac point and the reflection probability of electrons propagating along the quantum well. This paper is organized as follows. In Section 2, the theoretical model for the electrostatic potential is described. In Section 3, the spectrum of the confined states in the graphene asymmetric quantum well and the reflection properties are studied. The concluding remarks are given in Section 4.

2. Model

In monolayer graphene, the carriers near the Dirac points behave as mass-less particles and are governed by a 2D Dirac Hamiltonian[37,38] given by $v_{\mathrm{F}}(\boldsymbol{\sigma}\cdot\boldsymbol{p})$, where $v_{\mathrm{F}} = 10^6$ m·s^{-1} denotes the Fermi velocity, $\boldsymbol{\sigma} = (\sigma_x, \sigma_y)$ is the pseudospin matrix with components of the Pauli matrices, and $\boldsymbol{p} = (p_x, p_y)$ is the momentum operator. The model system we are interested in is a graphene asymmetric quantum well of width L (see Fig. 1) on the top of a substrate. The corresponding confining potential $V(x)$ is represented in the general form as follows:

$$V(x) = \begin{cases} V_{\mathrm{I}}, & x < 0, \\ V_{\mathrm{II}} = 0, & 0 \le x \le L, \\ V_{\mathrm{III}}, & x > L. \end{cases} \tag{1}$$

In the presence of one dimensional confining potential $V(x)$ and a substrate which induces a band gap that generates an effective mass like term mv_{F}^2, the low energy properties of the carriers with energy E are described by the Dirac equation

$$\left[v_{\mathrm{F}}(\boldsymbol{\sigma}\cdot\boldsymbol{p}) + V(x) + mv_{\mathrm{F}}^2\sigma_z\right]\Psi = E\Psi, \tag{2}$$

where we have neglected the inter-valley coupling.[35,39] In a given valley, a single-electron wave function of graphene is described as two-component spinor[13,39–44] $\Psi = [\Psi_{\mathrm{A}}, \Psi_{\mathrm{B}}]^{\mathrm{T}}$ where Ψ_{A} and Ψ_{B} refer to the two sublattices in the two-dimensional honeycomb lattice of carbon atoms (A and B).

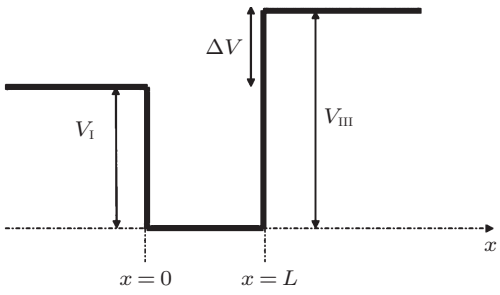


Fig. 1. Schematic diagram of the potential asymmetric quantum well.

Due to the translation invariance in the y direction, the motions in the x and y directions are decoupled and the solution can be written as $\Psi_{\mathrm{A}}(x,y) = \phi_{\mathrm{A}}(x)\,\mathrm{e}^{\mathrm{i}k_y y}$ an $\Psi_{\mathrm{B}}(x,y) = \phi_{\mathrm{B}}(x)\,\mathrm{e}^{\mathrm{i}k_y y}$, where k_y is the free component of the wave vector.

By introducing new dimensionless variables $\xi = x/L$, $\beta = k_y L$, $\varepsilon = EL/\hbar v_{\mathrm{F}}$, $u = V(x)L/\hbar v_{\mathrm{F}}$, and $\Delta = mv_{\mathrm{F}}^2 L/\hbar v_{\mathrm{F}}$, equation (2) takes the following dimensionless form:

$$\frac{\mathrm{d}\phi_{\mathrm{B}}(\xi)}{\mathrm{d}\xi} + \beta\phi_{\mathrm{B}}(\xi) = \mathrm{i}\,(\varepsilon - u - \Delta)\,\phi_{\mathrm{A}}(\xi), \tag{3a}$$

$$\frac{\mathrm{d}\phi_{\mathrm{A}}(\xi)}{\mathrm{d}\xi} - \beta\phi_{\mathrm{A}}(\xi) = \mathrm{i}\,(\varepsilon - u + \Delta)\,\phi_{\mathrm{B}}(\xi). \tag{3b}$$

These equations can be decoupled and formally written as

$$\frac{\mathrm{d}^2\phi_{\mathrm{A}}(\xi)}{\mathrm{d}\xi^2} + \frac{u'}{\varepsilon - u + \Delta}\frac{\mathrm{d}\phi_{\mathrm{A}}(\xi)}{\mathrm{d}\xi} - \left[\beta^2 + \beta\frac{u'}{(\varepsilon - u + \Delta)} - (\varepsilon - u)^2 + \Delta^2\right]\phi_{\mathrm{A}}(\xi) = 0, \tag{4}$$

where u' is the derivative of the potential. The analytical solution is obtainable for constant $u(x)$ and equation (4) becomes

$$\frac{\mathrm{d}^2\phi_{\mathrm{A}}(\xi)}{\mathrm{d}\xi^2} - f(\beta)\phi_{\mathrm{A}}(\xi) = 0, \tag{5}$$

where $f(\beta) = [\beta^2 - (\varepsilon - u)^2 + \Delta^2]$. Equation (5) does not have the form of the usual Schrödinger equation with potential u and eigenvalue ε. The behavior of the solution will depend on the sign of $f(\beta)$. The solutions may be real for $f(\beta) > 0$ and standing waves occur, and they may be complex for $f(\beta) < 0$ and traveling waves arise.

Recall that we study the case of a square asymmetric potential allowing $u(\xi)$ taking three different constant values, otherwise $f(\beta)$ admits three expressions having the same sign or different signs. Different possible combinations of $f(\beta)$ sign for the three regions I, II, and III allow us to construct an energy diagram showing the possible states of the carriers.

We show in Fig. 2 the energy diagram related to an asymmetric quantum well defined by $V_{\rm I} = 50$ meV, $V_{\rm II} = 0$ meV, $V_{\rm III} = 80$ meV, and $mv_{\rm F}^2 = 10$ meV. Zone boundaries E_0, E_1, E_2, E_3, and E_4 appearing in Fig. 2 correspond to $f(\beta) = 0$ and are given by $E_0 = \sqrt{(\hbar v_{\rm F} k_y)^2 + (mv_{\rm F}^2)^2}$, $E_1 = V_{\rm I} + \sqrt{(\hbar v_{\rm F} k_y)^2 + (mv_{\rm F}^2)^2}$, $E_2 = V_{\rm I} - \sqrt{(\hbar v_{\rm F} k_y)^2 + (mv_{\rm F}^2)^2}$, $E_3 = V_{\rm III} + \sqrt{(\hbar v_{\rm F} k_y)^2 + (mv_{\rm F}^2)^2}$, and $E_4 = V_{\rm III} - \sqrt{(\hbar v_{\rm F} k_y)^2 + (mv_{\rm F}^2)^2}$. Curves E_0 and E_1 delimit electron confined states respectively from the prohibited area and the semi-diffusive electron continuum. The curve E_4 introduces a cutoff in the spectrum at low wave vectors that arises due to the electron–hole conversion at the barrier interfaces. In both cases, $k_{yA} < k_y < k_{yC}$ and $k_y > k_{yC}$, where A (C) is the intersection of curves E_1 and E_4 (E_0 and E_4), the electron seems to be confined in an effective symmetric quantum well whose barrier heights are respectively $E_1 - E_4$ and $V_{\rm I}$ and characteristics are given in Figs. 3(a) and 3(b).

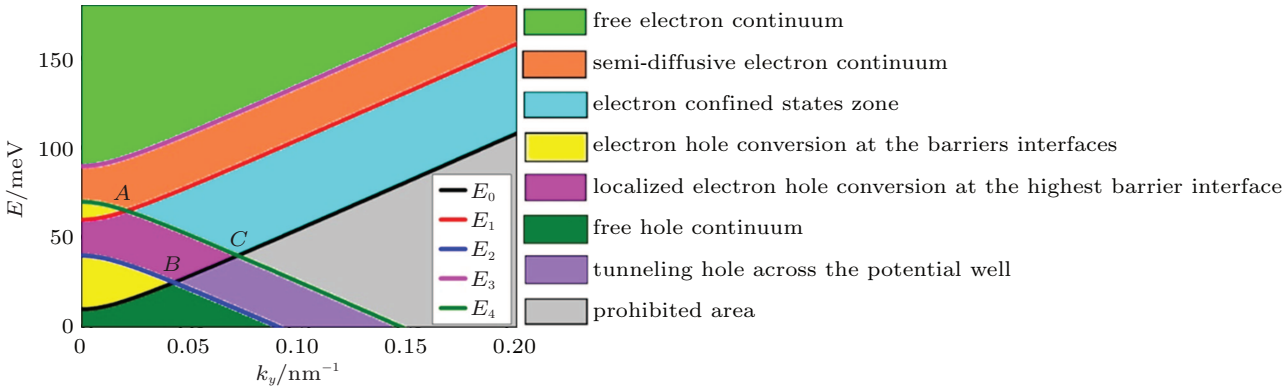


Fig. 2. (color online) Energy diagram related to an asymmetric well defined by $V_{\rm I} = 50$ meV, $V_{\rm II} = 0$, $V_{\rm III} = 80$ meV, and $L = 200$ nm. The energy gap induced by the substrate is $2mv_{\rm F}^2 = 20$ meV.

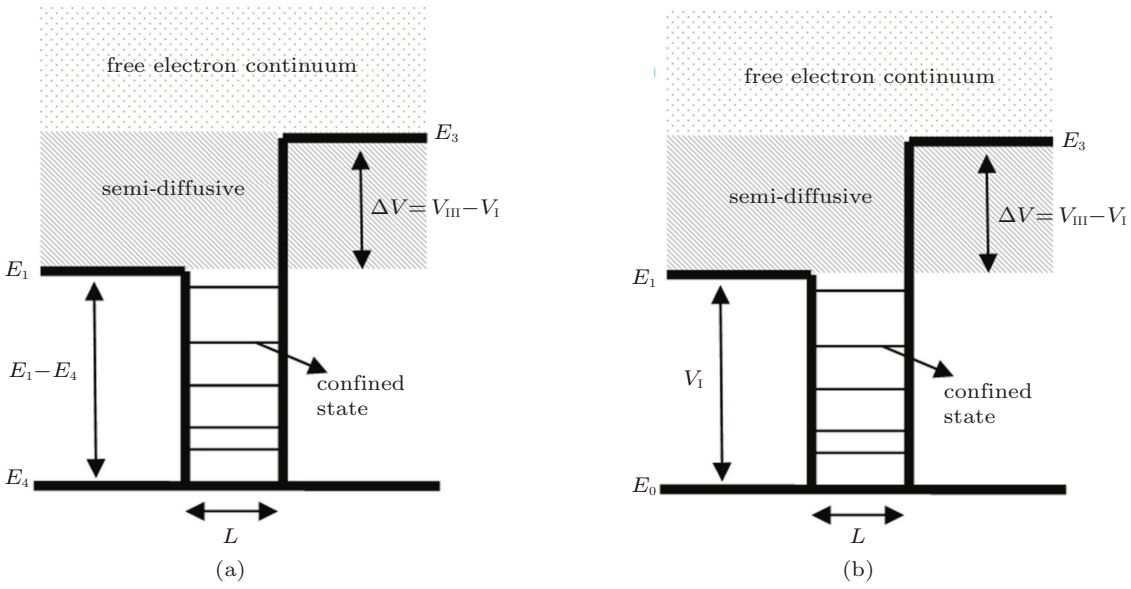


Fig. 3. (color online) (a) Effective quantum well for $k_{yA} < k_y < k_{yC}$. (b) Effective quantum well for $k_y > k_{yC}$.

For $k_{yA} < k_y < k_{yC}$ (see Fig. 3(a)), the barrier height depends on the free component of the wave vector k_y and is given by $E_1 - E_4 = 2\sqrt{(\hbar v_{\rm F} k_y)^2 + \left(mv_{\rm F}^2\right)^2} - \Delta V$. The barrier height approaches $2\hbar v_{\rm F} k_y$ in the absence of coupling with the substrate when ΔV reaches zero, which explains the fact that the number of levels depends strongly on k_y.[22] Note that k_{yA} and k_{yC} are shifted to lower wave vectors where k_{yC} coincides with k_{yB} which is given by $V_{\rm I}/2\hbar v_{\rm F}$. B is the intersection of curves E_0 and E_2. In this case, at k_{yA} that approaches zero, the barrier height is zero or small enough, thus prohibiting the confinement of carriers, and this corresponds to the normal electron incidence which allows the electron to travel along the quantum well. The coupling with the substrate induces an energy gap of $2mv_{\rm F}^2$ that generates a potential barrier of height $2mv_{\rm F}^2 - \Delta V$ at $k_{yA} = 0$, where carriers find their non-relativistic behavior and quantized states appear at $k_y = 0$.

In contrast to the previous case, the barrier height for $k_y > k_{yC}$ (Fig. 3(b)) is constant and equals to $V_{\rm I}$. In both cases, the height of the barrier is independent of the width of the quantum well.

To better understand the physics of this system, we conduct a theoretical study using analytical and numerical calculations. We establish a transcendental equation that characterizes the confined states. Electron semi-diffusive continuum and free electron continuum are characterized by an electronic reflection coefficient.

For the confined states, the spinor components decay exponentially in regions I and III. The A component of the spinor takes the following form:

$$\phi_{\rm A}(\xi) = \begin{cases} A_1 \mathrm{e}^{\alpha_1 \xi}, & \xi < 0, \\ B_1 \cos(\alpha_2 \xi) + B_2 \sin(\alpha_2 \xi), & 0 < \xi < 1, \\ A_3 \mathrm{e}^{-\alpha_3 \xi}, & \xi > 1, \end{cases} \tag{6}$$

with

$$\alpha_1 = \sqrt{\beta^2 - (\varepsilon - u_0)^2 + \Delta^2},$$
$$\alpha_2 = \sqrt{(\varepsilon - u_1)^2 - \beta^2 - \Delta^2},$$
$$\alpha_3 = \sqrt{\beta^2 - (\varepsilon - u_2)^2 + \Delta^2},$$

where $u_0 = V_{\rm I} L/\hbar v_{\rm F}$, $u_1 = V_{\rm II} L/\hbar v_{\rm F}$, and $u_2 = V_{\rm III} L/\hbar v_{\rm F}$.

From Eqs. (3b) and (6), $\phi_{\rm B}(\xi)$ can be given as

$$\phi_{\rm B}(\xi) = \begin{cases} \mathrm{i} A_1 f_1 \mathrm{e}^{\alpha_1 \xi}, & \xi < 0, \\ \dfrac{\mathrm{i}}{\varepsilon - u_1 + \Delta} \{B_1 [\beta \cos(\alpha_2 \xi) \\ + \alpha_2 \sin(\alpha_2 \xi)] \\ + B_2 [-\alpha_2 \cos(\alpha_2 \xi) \\ + \beta \sin(\alpha_2 \xi)]\}, & 0 < \xi < 1, \\ \mathrm{i} A_3 f_3 \mathrm{e}^{-\alpha_3 \xi}, & \xi > 1, \end{cases} \tag{7}$$

with

$$f_1 = \frac{\beta - \alpha_1}{\varepsilon - u_0 + \Delta},$$
$$f_3 = \frac{\beta + \alpha_3}{\varepsilon - u_2 + \Delta}.$$

By conducting a study similar to Pereira *et al.*'s work,[22] we derive the transcendental equation

$$S_1 (S_3 \sin(\alpha_2) - \alpha_2 \cos(\alpha_2)) + \alpha_2 (S_3 \cos(\alpha_2) + \alpha_2 \sin(\alpha_2)) = 0, \tag{8}$$

where $S_1 = \beta - (\varepsilon - u_1 + \Delta) f_1$ and $S_3 = \beta - (\varepsilon - u_1 + \Delta) f_3$.

The spinor two-components of the propagating wave solutions at a given incident energy E are represented by

$$\phi_{\rm A} = \begin{cases} a_0 \mathrm{e}^{\mathrm{i} k_0 \xi} + b_0 \mathrm{e}^{-\mathrm{i} k_0 \xi}, & \xi \le 0, \\ a_1 \mathrm{e}^{\mathrm{i} k_1 \xi} + b_1 \mathrm{e}^{-\mathrm{i} k_1 \xi}, & 0 \le \xi \le 1, \\ a_2 \mathrm{e}^{\mathrm{i} k_2 \xi}, & \xi \ge 1, \end{cases} \tag{9}$$

$$\phi_{\rm B} = \begin{cases} \dfrac{-\mathrm{i}}{(\varepsilon - u_0 + \Delta)} [(\mathrm{i} k_0 - \beta) a_0 \mathrm{e}^{\mathrm{i} k_0 \xi} \\ - (\mathrm{i} k_0 + \beta) b_0 \mathrm{e}^{-\mathrm{i} k_0 \xi}], & \xi \le 0, \\ \dfrac{-\mathrm{i}}{(\varepsilon - u_1 + \Delta)} [(\mathrm{i} k_1 - \beta) a_1 \mathrm{e}^{\mathrm{i} k_1 \xi} \\ - (\mathrm{i} k_1 + \beta) b_1 \mathrm{e}^{-\mathrm{i} k_1 \xi}], & 0 \le \xi \le 1, \\ \dfrac{-\mathrm{i}}{(\varepsilon - u_2 + \Delta)} \left[(\mathrm{i} k_2 - \beta) a_2 \mathrm{e}^{\mathrm{i} k_2 \xi}\right], & \xi \ge 1, \end{cases} \tag{10}$$

where

$$k_0 = \sqrt{(\varepsilon - u_0)^2 - \beta^2 - \Delta^2},$$
$$k_1 = \sqrt{(\varepsilon - u_1)^2 - \beta^2 - \Delta^2},$$
$$k_2 = \sqrt{(\varepsilon - u_2)^2 - \beta^2 - \Delta^2}.$$

The reflection and transmission amplitudes across the graphene quantum well are given respectively by $r = b_0/a_0$ and $t = a_2/a_0$. Similarly to Mhamdi *et al.*'s work,[35] we derive the following expression for refection r:

$$r = \frac{r_{01} - \dfrac{r_{01}}{r_{10}} r_{12} \mathrm{e}^{2\mathrm{i} k_1}}{1 - r_{10}^* r_{12} \mathrm{e}^{2\mathrm{i} k_1}}, \tag{11}$$

where

$$r_{mn} = \frac{\dfrac{\varepsilon - u_n + \Delta}{\varepsilon - u_m + \Delta} (\mathrm{i} k_m - \beta) - (\mathrm{i} k_n - \beta)}{\dfrac{\varepsilon - u_n + \Delta}{\varepsilon - u_m + \Delta} (\mathrm{i} k_m + \beta) + (\mathrm{i} k_n - \beta)}.$$

Here r_{mn} and r_{mn}^* denote respectively the reflection amplitude and its complex conjugate for two neighboring regions labeled by m and n. Note that $m, n = 0, 1, 2$ label regions respectively defined by potentials $V_{\rm I}$, $V_{\rm II}$, and $V_{\rm III}$ appearing in Eq. (1).

The total reflection probability R is obtained by taking the square of the module of the reflection amplitude r given by Eq. (11) $R = |r|^2$, and the total transmission probability is given by $T = 1 - R$.

In the next section, we focus on presenting properties of confined, semi-diffusive, and free electron states, where we will analyze the effects of the effective mass, the width of the well, and the heights of the barriers.

3. Results

Equation (8) is solved numerically and the resulting confined state energy spectrum is shown in Fig. 4 for an asymmetric quantum well characterized by $V_{\rm I} = 50$ meV, $V_{\rm II} = 0$ meV, $V_{\rm III} = 80$ meV, and $L = 200$ nm. The graphene sheet is on the top of a substrate that induces an energy gap of 20 meV ($mv_{\rm F}^2 = 10$ meV) which is, in this case, less than the asymmetry $\Delta V = V_{\rm III} - V_{\rm I} = 30$ meV.

The confined states are allowed only for $k_y > k_{yA}$ and they show an unusual quasi-linear dependence on the free component of the wave vector k_y. Also note that the number of

levels depends on k_y for low and large wave vectors. This is due to the cutoff induced by the curves E_1 and E_4 delimiting the confined states from the continuum regions. For $k_y > k_{yC}$, the confined states become increasingly dense when increasing k_y and the dispersion branches are given approximately by $E(k_y) = \hbar v_F \sqrt{(n\pi/L)^2 + k_y^2 + (mv_F/\hbar)^2}$.

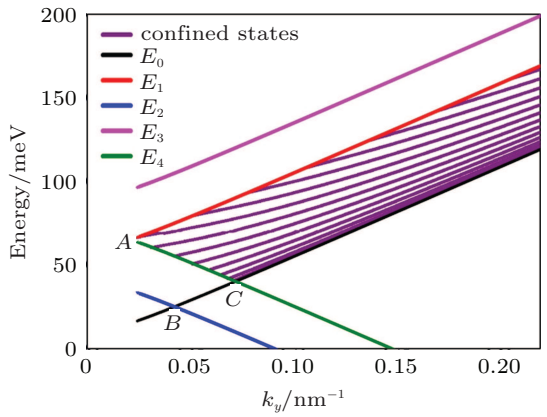


Fig. 4. (color online) Confined state energy spectrum for $V_I = 50$ meV, $V_{II} = 0$, $V_{III} = 80$ meV, $L = 200$ nm, and $mv_F^2 = 10$ meV.

The dispersion branches intercept curves E_1 and E_4 and a new class of confined states appears, mixed states, which refer at the same time to confined states and semi-diffusive electron states or free-hole states. Thus by an adiabatic increase of k_y, one can convert the carrier state from free-hole electron in a semi-diffusive state into a bound electron state. The general behavior of the confined states is similar to those in the presence of a symmetric quantum well potential,[22] where the limit of the electron–hole conversion is shifted to higher energies by ΔV which characterizes the asymmetry.

Now, we focus on the effect of the energy gap $2mv_F^2$ induced by the substrate when it exceeds the asymmetry ΔV. In Fig. 5, we plot the spectrum of the confined states for the same parameters as those in Fig. 4 while changing the substrate. In this case, we consider an energy gap of 53 meV ($mv_F^2 = 26.5$ meV). Figure 5 shows that the effective mass-like term mv_F^2 has a short range effect. Indeed, the effect of mv_F^2 is important for wave vectors smaller than k_{yC} where carriers have the non-relativistic behavior, and the quantized states appear at $k_y = 0$. This can be justified by studying the total reflection probability R under normal incidence ($k_y = 0$). In Fig. 6(a), we plot the variation of R with the incident energy for $k_y = 0$. For $mv_F^2 = 0$ and regardless of the asymmetry the coefficient R is always equal to zero, which is a signature of the Klein tunnelling.[26] When $mv_F^2 = 26.5$ meV and $\Delta V = 0$, which correspond to a symmetric quantum well, R reaches a series of minima. We notice that the minima, corresponding to the transparency, always reach zero. In this case, the transparency condition corresponds to the Fabry–Pérot resonance. Indeed, for a symmetric quantum well, the total reflection probability R takes the following expression:

$$R = \frac{4|r_{01}|^2 \sin^2(\alpha L)}{\{1 - |r_{10}|^2 \cos(2\alpha L)\}^2 + \{|r_{10}|^2 \sin(2\alpha L)\}^2}, \quad (12)$$

where

$$\alpha = \sqrt{\left(\frac{E}{\hbar v_F}\right)^2 - k_y^2 - \left(\frac{mv_F}{\hbar}\right)^2}.$$

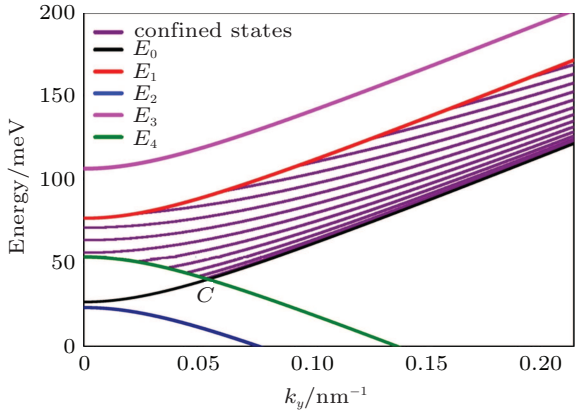
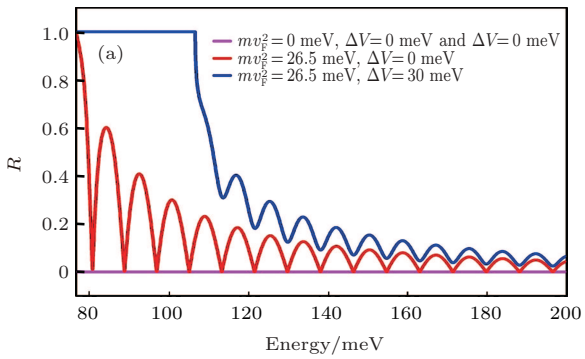


Fig. 5. (color online) Confined states energy spectrum for $V_I = 50$ meV, $V_{II} = 0$, $V_{III} = 80$ meV, $L = 200$ nm, and $mv_F^2 = 26.5$ meV.



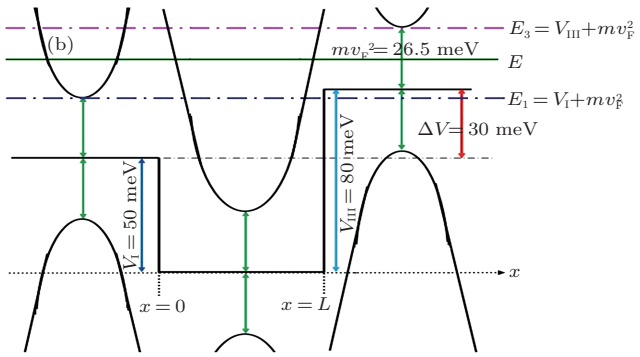


Fig. 6. (color online) (a) Total reflection probability R under normal incidence ($k_y = 0$) as a function of incident energy. The quantum well is defined by $V_I = 50$ meV, $V_{II} = 0$, $V_{III} = 50$ meV + ΔV, and $L = 200$ nm. The magenta curve corresponds to the two cases of ($mv_F^2 = 0$, $\Delta V = 0$) and ($mv_F^2 = 0$, $\Delta V = 30$ meV), the red curve to ($mv_F^2 = 26.5$ meV, $\Delta V = 0$), and the blue curve to ($mv_F^2 = 26.5$ meV, $\Delta V = 30$ meV). (b) Schematic diagrams of the spectrum carriers in monolayer graphene on the top of the h-BN substrate.

For $k_y = 0$, the perfect transparency condition is given by $\alpha L = n\pi$, where $\alpha = \sqrt{(E\hbar/v_F)^2 - (mv_F/\hbar)^2}$, which is the condition on the wave length $\lambda = 2\pi/\alpha = 2L/n$ usually associated to the Fabry–Pérot resonance. Then the interaction of the graphene sheet with the substrate induces an effective mass to the carriers, allowing the observation of the Fabry–Pérot resonance under normal incidence and the extinction of Klein tunnelling.

For a given asymmetry, the semi-diffusive continuum is located between curves $E_1 = V_I + \sqrt{(\hbar v_F k_y)^2 + (mv_F^2)^2}$ and $E_3 = V_{III} + \sqrt{(\hbar v_F k_y)^2 + (mv_F^2)^2}$. For $k_y = 0$, $E_1 = V_I + mv_F^2$ and $E_3 = V_{III} + mv_F^2$ and they are respectively 76.5 meV and 106.5 meV for $mv_F^2 = 26.5$ meV. As seen in Fig. 6(a), the asymmetry creates a transmission gap between the confined states and the free-electron continuum, wherein incident electrons with energies corresponding to the semi-diffusive continuum are completely reflected. This transmission gap characterizing the semi-diffusive continuum can be justified using a schematic diagram of the spectrum carriers in monolayer graphene on the top of the h-BN substrate (see Fig. 6(b)). In fact, an incident electron with energy E, located in the interval of the semi-diffusive states, is forbidden to pass to the region characterized by the potential V_{III} where no available states exist due to the gap induced by the substrate (see Fig. 6(b)).

The confined states that appear at zero k_y (see Fig. 5) belong to branches that do not intercept zones of the electron–hole conversion and the semi-diffusive electron continuum. For a given effective mass-like term mv_F^2, the number of confined states in the vicinity of $k_y = 0$ depends strongly on the asymmetry ΔV that induces a cutoff in the spectrum at low wave vectors. In Fig. 5, we notice that there are three confined states at $k_y = 0$ for $mv_F^2 = 26.5$ meV and $\Delta V = 30$ meV. This number increases to seven when ΔV reaches zero. In fact, when ΔV reaches zero, curve E_4 is shifted to lower energies to coincide with E_2 and all confined states with low energies are switched on. Then the asymmetry between the barriers can control the number of confined electrons. Furthermore, the main sources of decoherence are considerably weak, namely, the spin–orbit coupling and the hyperfine interaction. Therefore graphene on the the top of hexagonal boron nitride h-BN substrate can be exploited in the application of graphene quantum wells and quantum dots as logic states at the nanoscale.

For k_y higher than k_{yC}, the spectrum presents the same properties as those obtained in Fig. 4. The study of the total reflection probability R shows that an incident electron with an energy lying in the range of semi-diffusive energies is totally reflected as shown in Fig. 7 where we plot R as a function the electron incident energy for $k_y = 0.1\ \text{nm}^{-1} > k_{yC}$. Indeed, for a symmetric quantum well, the coefficient R oscillates with the incident energy and the minima attain zero. The particular energies corresponding to the transparency of the quantum well ($R = 0$) are given by

$$E(k_y) = \hbar v_F \sqrt{\left(\frac{n\pi}{L}\right)^2 + k_y^2 + \left(\frac{mv_F}{\hbar}\right)^2}.$$

The associated condition on the wave length is $\lambda' = 2\pi/\alpha' = 2L/n$, where $\alpha' = \sqrt{(n\pi/L)^2 + k_y^2 + (mv_F/\hbar)^2}$ corresponds to the Fabry–Pérot resonances. These Fabry–Pérot resonances become denser when increasing the width L of the quantum well, indicating that the quantum well possesses very dense confined states (see Figs. 8 and 9). The number of confined states depends on the width and the potential barrier height V_I. In fact, when $k_y > k_{yC}$ and for a given width L, the dispersion branches of confined states are approximately given by $E(k_y) = \hbar v_F \sqrt{(n\pi/L)^2 + k_y^2 + (mv_F/\hbar)^2}$. These confined states are situated between E_0 and E_1 given respectively by $\sqrt{(\hbar v_F k_y)^2 + (mv_F^2)^2}$ and $V_I + \sqrt{(\hbar v_F k_y)^2 + (mv_F^2)^2}$. Then by increasing the width L and the barrier height V_I, the confined states become more and more dense.

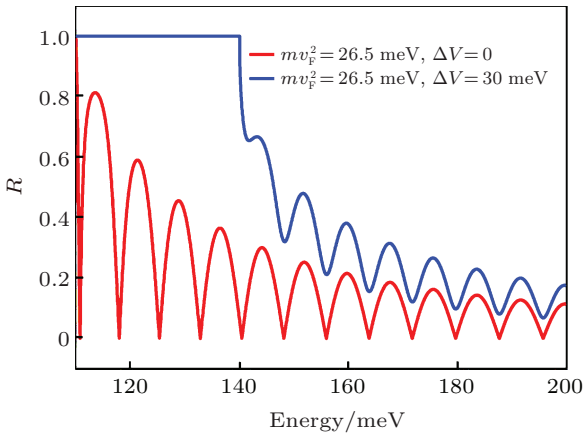


Fig. 7. (color online) Total reflection probability R under oblique incidence ($k_y = 0.1\ \text{nm}^{-1}$) as a function of incident energy. The quantum well is defined by $V_I = 50$ meV, $V_{II} = 0$, $V_{III} = 50$ meV + ΔV, and $L = 200$ nm. The red curve is for ($mv_F^2 = 26.5$ meV, $\Delta V = 0$) and the blue curve is for ($mv_F^2 = 26.5$ meV, $\Delta V = 30$ meV).

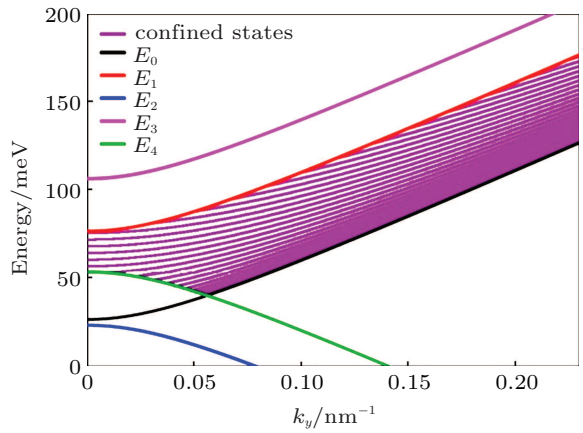


Fig. 8. (color online) Confined state energy spectrum for $V_I = 50$ meV, $V_{II} = 0$, $V_{III} = 80$ meV, $L = 400$ nm, and $mv_F^2 = 26.5$ meV.

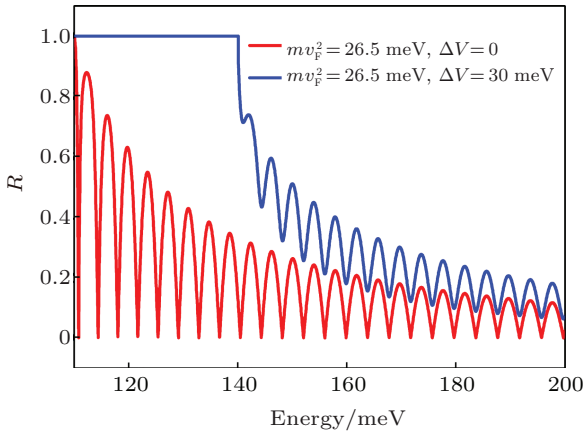


Fig. 9. (color online) Total reflection probability R under oblique incidence ($k_y = 0.1$ nm^{-1}) as a function of incident energy. The quantum well is defined by $V_{\rm I} = 50$ meV, $V_{\rm II} = 0$, $V_{\rm III} = 50$ meV + ΔV, and $L = 400$ nm. The red curve is for ($mv_{\rm F}^2 = 26.5$ meV, $\Delta V = 0$) and the blue curve is for ($mv_{\rm F}^2 = 26.5$ meV, $\Delta V = 30$ meV).

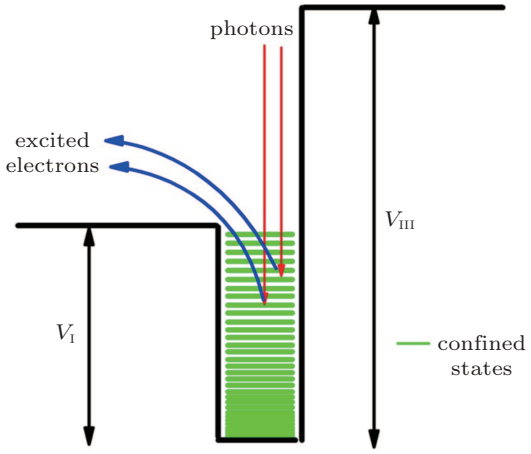


Fig. 10. (color online) Graphene asymmetric quantum well presenting very dense bound states and absorbing photons with different frequencies.

The presence of an asymmetry of 30 meV creates a transmission gap characterized by $R = 1$ (see Figs. 7 and 9). The transmission gap is situated between $E = 110.08$ meV and $E = 140.08$ meV that correspond to the limits of the semi-diffusive continuum when $k_y = 0.1$ nm^{-1}, $mv_{\rm F}^2 = 26.5$ meV, and $\Delta V = 30$ meV. For $E > 140.08$ meV, R goes through a series of minima that do not reach zero. These minima correspond to the same positions of the Fabry–Pérot resonances, indicating that the asymmetry does not affect the electron confined states.

This transmission gap opens the door for the application of graphene quantum wells as a photo-detector. Indeed, by absorbing a photon in a given frequency, an electron, occupying a bound state, is excited into a semi-diffusive state where it will be totally reflected and then be harvested from the side of the barrier $V_{\rm I}$ (see Fig. 10). The presence of very dense bound states indicates that the graphene quantum well can absorb photons with different frequencies to produce electricity. The barrier height $V_{\rm I}$ and the asymmetry ΔV determine the frequency operating regime of the photo-detector. For example, for far-infrared radiation at frequency between 0.3 THz and 20 THz, corresponding to the range from about 1.2 meV to 83 meV, $V_{\rm I}$ should be less than or equal to 83 meV so there would be enough numbers of electrons excited to the semi-diffusive continuum. The asymmetry ΔV should be larger than 83 meV to ensure that no electron escapes to the free electron continuum. Based on this example, we conclude that the asymmetry ΔV should be larger than the barrier height $V_{\rm I}$ (see Fig. 1). Note that this theoretical model is limited to low Fermi energies ($E < 1$ eV)[20] where the spectrum of quasi-particles in single-layer graphene is linear and modelled by the 2D Dirac Hamiltonian. Then this theoretical model can be extended only to the far infrared frequency regime.

4. Conclusion

We presented a theoretical study and numerical results on the electronic properties of a single-layer graphene asymmetric quantum well on the top of a substrate. The interaction with the substrate induces an effective mass-like term to carriers and quantized states appear around $k_y = 0$, where k_y is the free component of the wave vector. This effective mass-like term is characterized by the appearance of Fabry–Pérot resonances under normal incidence. The creation of an asymmetry between the barriers can control the number of confined states around $k_y = 0$. For a large quantum well and when k_y is larger than a given k_{yC}, the confined states are very dense, which implies that the graphene quantum well can absorb photons with different frequencies. The asymmetry creates a transmission gap between the confined states and the free electron continuum, and the excited electrons in the bound states to the semi-diffusive continuum are totally reflected and then harvested to produce electricity. The graphene asymmetric quantum well can be exploited as photo-detectors operating at far- and mid-infrared frequency regimes.

Acknowledgment

E. Ben Salem is grateful to J. N. Fuchs (LPS, Université Paris-Sud, bâtiment 510, F-91405 Orsay Cedex, France) and F. M. Peeters (University of Antwerp; Department of Physics; Groenenborgerlaan 171, B-2020 Antwerpen, Belgium) for helpful discussions.

References

[1] Geim A K and Novoselov K S 2007 *Nat. Mater* **6** 183
[2] Castro Neto A H, Guinea F, Peres N M R, Novoselov K S and Geim A K 2009 *Rev. Mod. Phys.* **81** 109
[3] Li X S, Cai W, An J Kim S, Nah J, Yang D, Piner R, Velamakanni A, Jung I, Tutuc E, Banerjee S K Colombo L and Ruoff R S 2009 *Science* **324** 1312
[4] Schwierz F 2010 *Nat. Nanotechnol.* **5** 487

[5] Han M Y, Özyilmaz B, Zhang Y and Kim P 2007 *Phy. Rev. Lett.* **98** 206805
[6] Rycerz A, Tworzydlo J and Beenakker C W J 2007 *Nat. Phys.* **3** 172
[7] Ponomarenko L A, Schedin F, Katsnelson M I, Yang R, Hill E W, Novoselov K S and Geim A K 2008 *Science* **320** 356
[8] Jiao L, Zhang L, Wang X, Diankov G and Dai H 2009 *Nature* **458** 877
[9] Kosynkin D V, Higginbotham A L, Sinitskii A, Lomeda J R, Dimiev A, Price B K James M and Tour J M 2009 *Nature* **458** 872
[10] Ritter K A and Lyding J W 2009 *Nat. Mater.* **8** 235
[11] Cai J, Ruffieux P, Jaafar R, Bieri M, Braun T, Blankenburg S, Muoth M, Seitsonen A P, Saleh M, Feng X, Müllen K and Fasel R 2010 *Nature* **466** 470
[12] Sprinkle M, Ruan M, Hu Y, Hankinson J, Rubio-Roy M, Zhang B, Wu X, Berger C and de Heer W A 2010 *Nat. Nanotechnol.* **5** 727
[13] Trauzettel B, Bulaev D V, Loss D and Burkard G 2007 *Nat. Phys.* **3** 192
[14] Mak K F, Ju L, Wang F and Heinz T F 2012 *Solid State Commun.* **152** 1341
[15] Nair R R, Blake P, Grigorenko A N, Novoselov K S, Booth T J, Stauber T, Peres N M R and Geim A K 2008 *Science* **320** 1308
[16] Rogalski A 2003 *Prog. Quant. Electron* **27** 59
[17] Clark J and Lanzani G 2010 *Nat. Photon.* **4** 438
[18] Rodrigo D, Limaj O, Janner D, Etezadi D, Abajo F J G, Pruneri V and Altug H 2015 *Science* **34** 165
[19] Liu C H, Chang Y C, Norris T B an Zhong Z 2014 *Nat. Nanotechnol.* **9** 273
[20] Katsnelson M I, Novoselov K S and Geim A K 2006 *Nat. Phys.* **2** 620
[21] Min H, Hill J E, Sinitsyn N A, Sahu B R, Kleinman L and MacDonald A H 2006 *Phys. Rev. B* **74** 165310
[22] J. Milton Pereira Jr J M, Mlinar V and Peeters F M 2006 *Phys. Rev. B* **74** 045424
[23] Williams J R, Low T, Lundstrom M S and Marcus C M 2011 *Nat. Nanotechnol.* **6** 222
[24] Thornton T J, Pepper M, Ahmed H, Andrews D and Davies G J 1986 *Phys. Rev. Lett.* **56** 1198
[25] Zheng H Z, Wei H P, Tsui D C and Weimann G 1986 *Phys. Rev. B* **34** 5635
[26] Giovannetti G, Khomyakov P A, Brocks G, Kelly P J and Brink J V D 2007 *Phys. Rev. B* **76** 073103
[27] Suenaga K, Colliex C, Demoncy N, Loiseau A, Pascard H and Willaime F 1997 *Science* **278** 653
[28] Skomski R, Dowben P A, Driver M S and Kelber J A 2014 *Mater. Horiz.* **1** 563
[29] Gorbachev R V, Song J C W, Yu G L, Kretinin A V, Withers F, Cao Y, Mishchenko A, Grigorieva I V, Novoselov K S, Levitov L S and Geim A K 2014 *Science* **346** 448
[30] Hwang E H, Adam S and Sarma S D 2007 *Phys. Rev. Lett.* **98** 186806
[31] Adam S, Hwang E H, Galitski V and Sarma S D 2007 *Proc. Natl. Acad. Sci. USA* **104** 18392
[32] Martin J, Akerman N, Ulbricht G, Lohmann T, Smet J H, von Klitzing K and Yacoby A 2008 *Nat. Phys.* **4** 144
[33] Xue J, Sanchez-Yamagishi J, Bulmash D, Jacquod P, Deshpande A, Watanabe K, Taniguchi T, JarilloHerrero P and LeRoy B J 2011 *Nat. Mater.* **10** 282
[34] Dean C R, Young A F, Meric I, Lee C, Wang L, Sorgenfrei L, Watanabe K, Taniguchi T, Kim P, Shepard K L and Hone J 2010 *Nat. Nanotechnol.* **5** 722
[35] Mhamdi A, Ben Salem E and Jaziri S 2013 *Solid State Commun.* **175** 106
[36] Wang J T, Guo D S, Zhao G L, Chen J C, Sun Z W and Ignatiev A 2013 *WJCMP* **3** 67
[37] Slonczewski J C and Weiss P R 1958 *Phys. Rev.* **109** 272
[38] Semenoff G W 1984 *Phys. Rev. Lett.* **53** 2449
[39] Allain P E and Fuchs J N 2011 *Eur. Phys. J. B* **83** 301
[40] Brey L and Fertig H A 2006 *Phys. Rev. B* **73** 235411
[41] Novoselov K S, Geim A K, Morozov S V, Jiang D, Zhang Y, Dubonos S V, Grigorieva I V and Firsov A A 2004 *Science* **306** 666
[42] Novoselov K S, Geim A K, Morozov S V Jiang D, Katsnelson M I, Grigorieva I V, Dubonos S V and Firsov A A 2005 *Nature* **438** 197
[43] Zhang Y, Tan Y W, Stormer H and Kim P 2005 *Nature* **438** 201
[44] Berger C, Song Z, Li X, Wu X, Brown N, Naud C, Mayou D, Li T, Hass J, Marchenkov A N, Conrad E H, First P N and de Heer W A 2006 *Science* **312** 1191